

USING TIME-SERIES SATELLITE IMAGERY TO DETECT ARTIFICIAL LIGHT AT NIGHT: THE CASE OF LUOJIA-1 AND INTERNATIONAL SPACE STATION

Shengjie Kris LIU^{1,2}, Chu Wing SO¹, Jason Chun Shing PUN¹

¹Department of Physics, The University of Hong Kong, Pokfulam, Hong Kong

²Spatial Sciences Institute, University of Southern California, Los Angeles, CA, USA

ABSTRACT

Artificial light at night (ALAN) changes throughout the night and the year within an area. It is crucial to monitor the time-series characteristics of ALAN. In this study, we investigated the changes in ALAN in Hong Kong over time from two medium-resolution remote sensing products: Luojia 1-01 (LJ-1) and the International Space Station (ISS). We validated these images with in-situ night sky brightness measurements. The results show that both the calibrated LJ-1 and the uncalibrated ISS images achieved similar agreements with the in-situ data ($R=0.73$ and $R=0.83$, respectively). LJ-1 and ISS images are useful for evaluating ALAN changes over the years and throughout the night, respectively. In early nights (before 23:00), commercial areas were brighter, while in late nights (after 23:00), port facilities and airports were brighter. Finally, we highlight the importance of color composition, time-series observations within one night, and multi-angle observations within minutes for ALAN monitoring.

Index Terms— Artificial light at night, nighttime light remote sensing, Luojia-1, International Space Station, multiple angle

1. INTRODUCTION

The civilization process of human society shapes the Earth environment. As a result, about 3% of the Earth's land surface has been urbanized [1]. These urban areas emit artificial light at night (ALAN) to the surroundings, leading to a brightened night sky. With the skyrocketing light pollution, 99% of the world population is living under a light-polluted night sky [2, 3]. More than half of the populations in the U.S. and Europe can no longer see the Milky Way with naked eyes [4].

Continuous time-series monitoring is critical to evaluate light pollution. On Earth, sensors such as the sky quality meter (SQM) have been used to establish monitoring networks

E-mails: liusheng@usc.edu (SKL), socw@connect.hku.hk (CWS), jcsun@hku.hk (JCSP). This work was supported in part by the Environment and Conservation Fund (Project ID: 2018-125) of the Government of the Hong Kong Special Administrative Region, and in part by The University of Hong Kong Knowledge Exchange Fund granted by the University Grants Committee (KE-IP-2019/20-54, KE-IP-2020/21-78) of the University of Hong Kong.

around the world [3, 5, 6, 7]. In space, sensors onboard satellites orbit the Earth every night to capture ALAN, such as the Visible Infrared Imaging Radiometer Suite (VIIRS) instruments onboard the Suomi National Polar-Orbiting Partnership (Suomi NPP) spacecraft. The International Space Station (ISS) – commonly recognized as the largest man-made satellite – also captures nighttime imagery occasionally [8]. Unlike common satellite products, such as those from VIIRS and LJ-1, ISS images are not limited to a specific local passing time and thus have the potential to record ALAN throughout the night. ISS images are also one of the few nighttime color image sources dating back to the 2000s, with a spatial resolution of ~ 100 meters depending on the focal length of the camera. While VIIRS provides continuous time-series monitoring, the spatial resolution of 750 meters is somehow limited. New nano satellites, such as LJ-1 launched in 2018 [9], provide observations close to ~ 100 meters, similar to those from ISS.

In this paper, we collected time-series LJ-1 and ISS images over Hong Kong to study the changes of ALAN over time. We also validated these observations in terms of their agreements with the night sky brightness (NSB) taken from sky quality meters from the Globe at Night - Sky Brightness Monitoring Network (GaN-MN) [7].

2. DATA AND METHOD

2.1. Images from ISS and LJ-1

Table 1 shows the information (acquisition date, time, and number of snapshots) of the four sets of ISS images and four sets of LJ-1 images, respectively. For each set, because the satellite continuously takes images during its orbiting and each image alone is still large enough to include the study area, there are multiple snapshots within minutes that we can use. As light emission is highly directional, these snapshots provide a natural solution of multiple-angle observations of ALAN [10]. We included all these images in the analysis.

ISS images have no projection information and require additional processing. We obtained the raw-format ISS image files in 16 bit and georeferenced them using the ArcGIS software. By selecting a number of control points between

Table 1. Acquisition date, time, and number of snapshots of the four sets of ISS and four sets of LJ-1 images.

Source	Date	Snapshots	Local Time
ISS	20150119	7	0:57:46 ⁺¹ -0:58:25 ⁺¹
ISS	20150123	13	23:07:22-23:08:19
ISS	20180228	6	4:35:42 ⁺¹ -4:36:05 ⁺¹
ISS	20200226	2	3:32:36 ⁺¹ -3:32:37 ⁺¹
LJ-1	20180903	6	22:44:02-22:44:27
LJ-1	20181124	5	22:46:52-22:47:12
LJ-1	20190129	6	22:56:32-22:56:57
LJ-1	20190311	2	22:56:18-22:56:23

twenties and forties, depending on the image, with the visual inspection on high-resolution optical images and the OpenStreetMap road network as references, we obtained the georeferenced images using the third-order polynomial interpolation. The root mean square errors (RMSE) of the georeferenced images were roughly between 66 and 196 meters. All ISS images were interpolated to a spatial resolution of 111 meters using the bilinear interpolation algorithm. Fig. 1 shows sample ISS and LJ-1 nighttime images and one Sentinel-2 daytime image. No radiometric calibration was done on ISS images due to a lack of information.

2.2. Calibration of LJ-1 images

To calibrate LJ-1 images, we converted the raw digital number (DN) values to at-sensor radiance using the equation provided by the data provider [9]:

$$L = 10^{-10} d^{3/2} \quad W/(m^2 \cdot sr \cdot \mu m), \quad (1)$$

where L and d are at-sensor radiance and raw DN value, respectively. The radiance data were then multiplied by 10^5 in our study so that the data range is roughly 0-10,000.

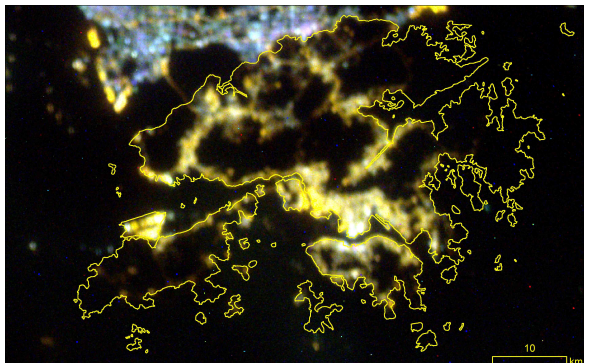
2.3. Night sky brightness data

Night sky brightness (NSB) data were obtained from the GaN-MN¹, which was launched since 2014. Each sensor (sky quality meter) takes a measurement every 30 seconds. There were seven available stations in Hong Kong during the time of image acquisition (with additional three from a nearby city, Macau). The NSB data were processed to exclude sunlight, moonlight, and other abnormal values. The NSB value is in logarithmic scale; a larger value indicates a darker sky. For visualization, we plot the figures with smaller values on top (brighter) and larger values in the bottom (darker), consistent with the current literature [5]. Fig. 2 shows the sample NSB measurements from one night. The NSB value often ranges from 14 to 23 mag/arcsec². A dark sky without light pollution should be darker than 21.6 mag/arcsec².

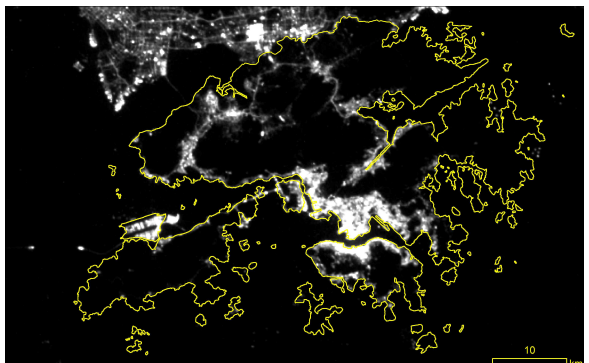
¹<http://globeatnight-network.org/global-at-night-monitoring-network.html>



(a) Sentinel-2 daytime image in 2020



(b) ISS-20150119, 0:58:25⁺¹



(c) LJ-1-20190311, 22:56:18

Fig. 1. Sample images from Sentinel-2 (daytime 2020), ISS (20150119, 0:58:25⁺¹), and LJ-1 (20190311, 22:56:18)

Measurement of NSB is highly sensitive through the sky quality meter. A big factor affecting NSB is clouds. When it is cloudy, the back-scattered ALAN from clouds in the night sky becomes strong, brightening the night sky. When this happens, the exact value of NSB is also fluctuated due to the changing cloud fraction. In a near cloudless condition, the scattering effect of ALAN turns weak, darkening the night sky. In the sample NSB data shown in Fig. 2, it was a relatively cloudless night. At 23:00, a sudden decrease of the brightness happened, which was a result due to many ex-

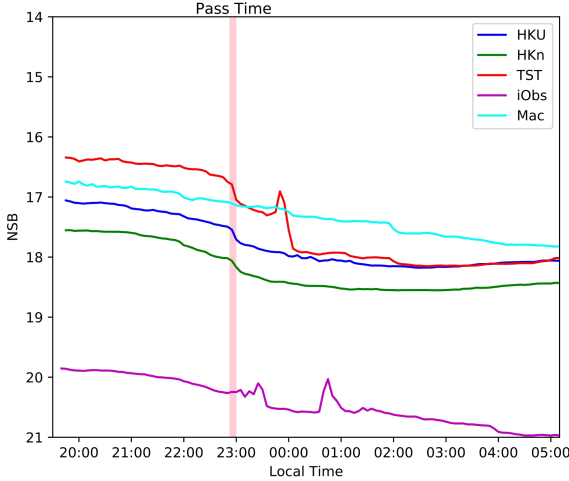


Fig. 2. Sample NSB data on 2019-03-11. NSB unit is mag/arcsec², the larger the darker.

ternal decorative lights were turned-off at this time following the guidance from the Charter on External Lighting in Hong Kong and the International Commission on Illumination (CIE) [11].

2.4. Land use data

Land use data of 2018 are from the Planning Department. The original land use data are organized using a two-level classification system. A total of 10 classes with 27 subclasses are available. We grouped them into 14 categories in our study, as shown Table 2. These 14 land use classes are private residential, public residential, rural settlement, commercial, industrial, institutional open space, roads and railways, airport, port facilities, other urban, agriculture, natural vegetation, barren, and water bodies.

Table 2. Land use data.

Land use class	Number of pixels
Private Residential	2291
Public Residential	1478
Rural Settlement	2998
Commercial	389
Industrial	2291
Institutional Open Space	4742
Roads and Railways	4501
Airport	1127
Port Facilities	404
Other Urban	3900
Agriculture	5862
Natural Vegetation	64174
Barren	533
Water Bodies	2692

3. RESULTS

3.1. Validation of ISS and LJ-1 images with NSB

Figure 3 shows the scatter plots between NSB and LJ-1 images and between NSB and ISS images, respectively. Overall, the uncalibrated ISS images have a better agreement with the in-situ NSB measurement ($R=0.8309$), and the calibrated LJ-1 images with a lesser agreement ($R=0.7282$). In terms of multiple snapshots, the values on ISS images and LJ-1 images changed by almost 1 unit (logarithmic scale) in some cases. As the images are almost cloud free, these changes are largely due to the changing observation angle.

3.2. ALAN by land use

We examine the average brightness of land use categories through a time-series fashion and show them in order, as shown in Fig. 4. For the relative brightness and ranking from LJ-1, both the mean values and ranking are relatively stable. Commercial areas are the brightest, followed by port facilities, roads and railways, and airport. Natural land use classes are with the lowest brightness as expected.

Because the local pass time is different for ISS images, we are able to get more information from them. Commercial areas were the brightest at 23:08, the brightness dropped in late nights, at 0:58, 3:32 and 4:36, to the 4th brightest land use class. In late nights, port facilities and airport were the brightest. At 4:36, public residential areas were even slightly brighter than commercial areas.

4. CONCLUSION

We reported the preliminary result of using ISS and LJ-1 images to examine the ALAN changes over Hong Kong. These images achieved good agreements with the in-situ NSB data ($R=0.73$ and $R=0.83$). With the time-series ISS images, we are able to track the ALAN changes of different land use over night.

5. REFERENCES

- [1] Karen C Seto, Burak Güneralp, and Lucy R Hutyra, “Global forecasts of urban expansion to 2030 and direct impacts on biodiversity and carbon pools,” *Proceedings of the National Academy of Sciences*, vol. 109, no. 40, pp. 16083–16088, 2012.
- [2] Fabio Falchi and Salvador Bará, “Light pollution is skyrocketing,” *Science*, vol. 379, no. 6629, pp. 234–235, 2023.
- [3] Christopher CM Kyba, Yiğit Öner Altıntaş, Constance E Walker, and Mark Newhouse, “Citizen scientists report global rapid reductions in the visibility of stars from 2011 to 2022,” *Science*, vol. 379, no. 6629, pp. 265–268, 2023.
- [4] Pierantonio Cinzano, Fabio Falchi, and Christopher Elvidge, “The first world atlas of the artificial night sky brightness,”

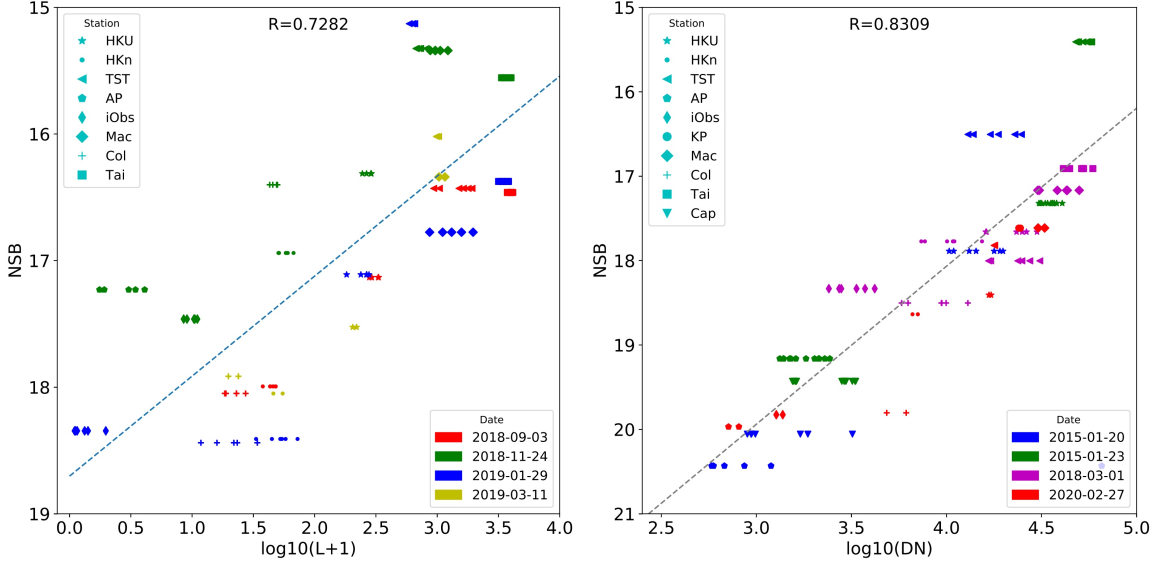


Fig. 3. Scatter plots between NSB and LJ-1 ($R=0.7282$) and NSB and ISS ($R=0.8309$). The dash line is the best-fit line.

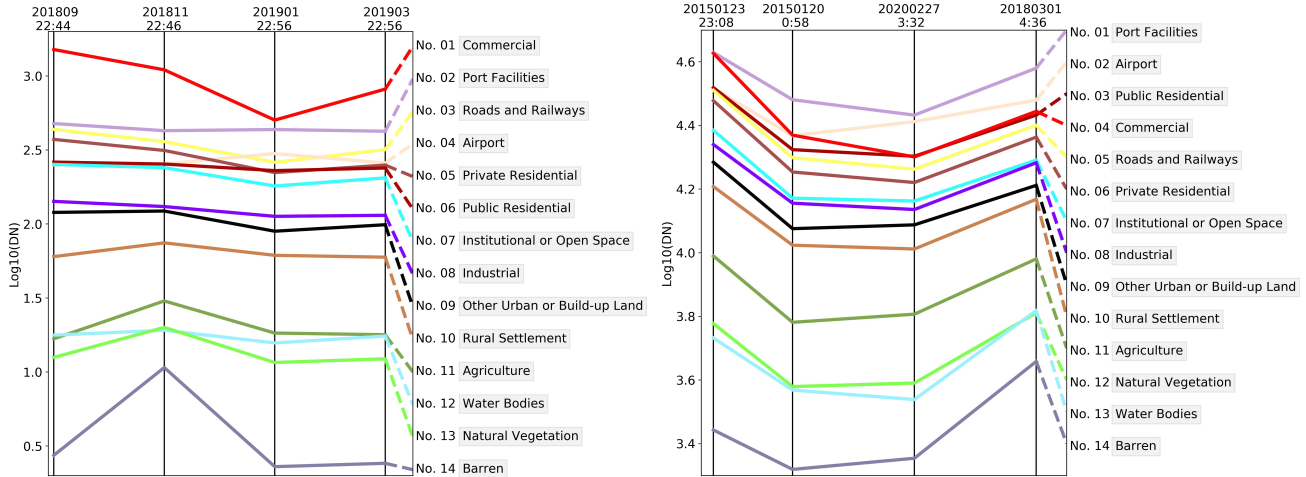


Fig. 4. ALAN ranking by land use from LJ-1 (left) and ISS (right). The ranking order is based on the log-scale value (y-axis) averaged from the land use type. The dash line links the log-scale value to the relative ranking.

- Mon. Notices Royal Astron. Soc.*, vol. 328, no. 3, pp. 689–707, 2001.
- [5] Chun Shing Jason Pun and Chu Wing So, “Night-sky brightness monitoring in Hong Kong,” *Environmental monitoring and assessment*, vol. 184, no. 4, pp. 2537–2557, 2012.
- [6] John C Barentine, “Night sky brightness measurement, quality assessment and monitoring,” *Nature Astronomy*, vol. 6, no. 10, pp. 1120–1132, 2022.
- [7] Chun Shing Jason Pun, Chu Wing So, Wai Yan Leung, and Chung Fai Wong, “Contributions of artificial lighting sources on light pollution in Hong Kong measured through a night sky brightness monitoring network,” *J. Quant. Spectrosc. Radiat. Transf.*, vol. 139, pp. 90–108, 2014.
- [8] Alejandro Sánchez de Miguel et al., “Colour remote sensing of the impact of artificial light at night (i): The potential of the international space station and other dslr-based platforms,” *Remote Sens. Environ.*, vol. 224, pp. 92–103, 2019.
- [9] Xi Li, Xiya Li, Deren Li, Xiaojun He, and Michael Jendryke, “A preliminary investigation of luojia-1 night-time light imagery,” *Remote Sens. Lett.*, vol. 10, no. 6, pp. 526–535, 2019.
- [10] Christopher Kyba et al., “Multiple angle observations would benefit visible band remote sensing using night lights,” *J. Geophys. Res. Atmos.*, vol. 127, no. 12, pp. e2021JD036382, 2022.
- [11] Tin Fai Kwok, Yuan Xu, and Pui Ting Wong, “Complying with voluntary energy conservation agreements (ii): lighting in Hong Kong’s shopping malls,” *Resources, Conservation and Recycling*, vol. 117, pp. 225–234, 2017.